Cryo-EM Facility at SOLARIS — A Highlight Review of Complex Biological Assemblies

G. Ważny[a,b], P. Indyka[a], M. Rawski[a], M. Jaciuk[a] and A.P. Biela[a,*]

[a] *SOLARIS National Synchrotron Radiation Centre, Jagiellonian University, Czerwone Maki 98, 30-392 Kraków, Poland*
[b] *Doctoral School of Exact and Natural Sciences, Jagiellonian University, S. Łojasiewicza 11, 30-348 Kraków, Poland*

Received: 15.01.2026 & Accepted: 04.05.2026

Doi: 10.12693/APhysPolA.149.S167 *e-mail: artur.biela@uj.edu.pl

Cryo-electron microscopy has emerged as a transformative technique in structural biology, enabling the high-resolution structural determination of large and heterogeneous biological assemblies. This review highlights recent advances in understanding the structural and functional diversity of protein cages, ribonucleic acid molecules and complexes, as well as enzyme complexes, as revealed by cryo-electron microscopy. We discuss how cryo-electron microscopy provides unique insights into the architecture, dynamics, and mechanisms of action of these essential biological components.

topics: cryo-electron microscopy (cryo-EM), structural biology, biological assemblies, ribonucleic acid (RNA)

1. Introduction

Structural biology is fundamental to elucidating the intricate mechanisms underlying life's processes. Determining the three-dimensional arrangement of biomolecule atoms and interactions allows researchers to decipher the functional consequences of specific structural features, dynamic conformational changes, and regulatory mechanisms. While X-ray crystallography and nuclear magnetic resonance (NMR) spectroscopy have long been cornerstones of structural biology, cryo-electron microscopy (cryo-EM) has undergone a profound technological and methodological transformation, often referred to as the "resolution revolution," driven by advancements in direct electron detectors technology, improved sample vitrification strategies, sophisticated image processing algorithms, and increasing levels of instrumentation automation [1, 2]. This has enabled the determination of high-resolution structures of increasingly complex biological assemblies, often bypassing the need for crystallization, which is a major limitation of X-ray crystallography, and restriction of molecule size — the main constraint of NMR. Consequently, these developments enable the cryo-EM method to become an indispensable tool for the routine determination of near-atomic- and atomic-resolution structures of a wide range of biological macromolecules, including protein complexes [3], ribosomes [4], viruses [5], and membrane proteins [6].

Despite its transformative impact, cryo-EM intrinsically relies on the interaction of high-energy electrons with radiation-sensitive biological specimens, making radiation damage a fundamental limitation of the technique. Electrons interact with the sample through two principal mechanisms, i.e, elastic and inelastic scattering. Elastically scattered electrons are deflected by the electrostatic potential of the sample without energy loss and are responsible for generating the image contrast between the biological material and the surrounding vitreous ice. In contrast, inelastic scattering events involve partial energy deposition within the sample, leading to excitation and ionization processes that contribute directly to radiation-induced damage and degradation of structural integrity. Notably, the ratio of damaging (inelastic) to non-destructive (elastic) interactions is estimated to be approximately $3:1$ [7], underscoring the intrinsic vulnerability of biological specimens to electron irradiation.

Radiation damage in cryo-EM is commonly described as a multistage process. Primary damage results from the direct interaction of incident high-energy electrons with the sample, causing ionization, bond breaking, and the generation of secondary electrons and reactive free radicals. Secondary damage follows as these secondary electrons and free radicals migrate through the specimen interior, initiating a cascade of chemical reactions that amplify both structural and chemical alterations. Finally, tertiary damage manifests through the accumulation of molecular hydrogen

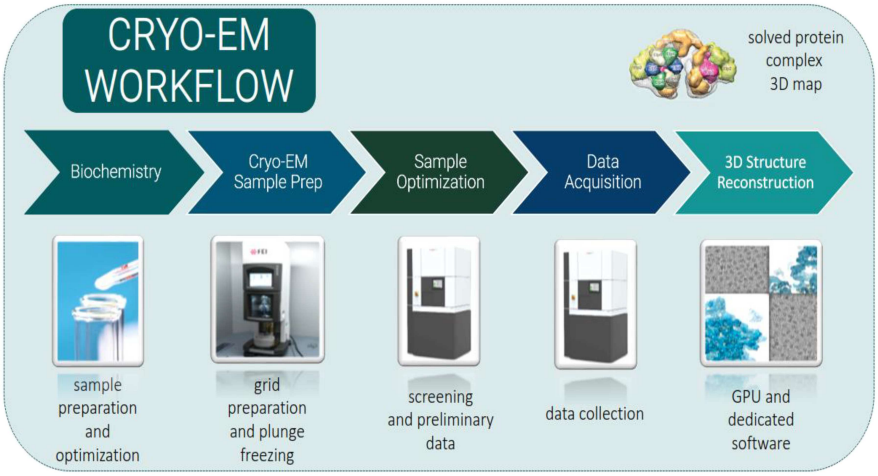

Fig. 1. The cryo-EM workflow presenting five essential stages of a standard cryo-EM SPA or cryo-ET experiment.

within the sample, leading to pronounced morphological changes such as bubbling or mass loss. Together, these processes progressively erode high-resolution structural information during data acquisition.

To mitigate beam-induced damage while preserving sufficient image contrast, careful control of the total electron dose is essential [8]. In practice, this involves optimizing imaging conditions to balance signal-to-noise ratio against structural preservation. A standard strategy for dose control is adjustment of the exposure time per movie, thereby regulating the total number of electrons that interact with the specimen during data collection. Such dose-fractionation strategies are now a central component of modern cryo-EM workflows and are critical for maximizing the achievable resolution of radiation-sensitive biological samples.

This review highlights recent cryo-EM-derived structural findings generated in collaboration with the National Synchrotron Radiation Centre (NSRC) SOLARIS Cryo-EM Facility. For clarity, the reported results are grouped into three major categories of biological molecules and assemblies: (i) protein cages, both natural and artificial; (ii) ribonucleic acid (RNA) and its modifications; and (iii) enzyme complexes. We explore the diversity in size, architecture, and molecular mechanisms revealed by recent cryo-EM studies, drawing attention to the wide range of biological systems that can now be visualized with unprecedented clarity. We emphasize the importance of high-resolution structures in elucidating molecular interactions, conformational changes, and regulatory pathways. Access to near-atomic details allows researchers to infer essential information about the behavior and functionality of investigated macromolecules. The overarching goal of this work is to provide a comprehensive overview of the structural and functional knowledge gained through cryo-EM, highlighting recent progress. By showcasing structural and functional diversity, we aim not only to summarize current developments but also to inspire further research in this rapidly evolving field. Ultimately, demonstrating the strengths of cryo-EM underscores its potential to unravel the complexities of biological systems at multiple levels of organization, thereby paving the way for new therapeutic strategies, diagnostic tools, and biotechnological innovations.

2. SOLARIS Cryo-EM Facility infrastructure

2.1. Experiments using SOLARIS equipment

The standard cryo-EM experiment encompasses multiple steps, including sample preparation, sample vitrification, grid screening, high-resolution data collection, and data processing with reconstruction of three-dimensional (3D) potential maps of the sample. Figure 1 presents the scheme of the cryo-EM workflow. The sample can be prepared in a biological or biochemical laboratory and pre-characterized with the use of common methods such as denaturing polyacrylamide gel electrophoresis (SDS-PAGE), size-exclusion chromatography (SEC), native mass spectrometry (nMS), dynamic light scattering (DLS), etc. The ideal candidate sample for a cryo-EM experiment should be of very high purity, monodispersed ($> 99\%$, i.e., single band on an SDS-PAGE gel), and have low conformational heterogeneity (ideally locked in one catalytic state). The ideal buffer composition should be of low-to-moderate ionic strength (0–150 mM NaCl) and should not contain or contain only very low levels of cryo-protectants (i.e., $< 2\%$ of glycerol). Such a sample has the potential to provide a high-resolution cryo-EM reconstruction. To

TABLE I
Specification of Krios G3i and Glacios cryo-electron microscopes used in SOLARIS Cryo-EM Facility.

Parameter	Value	
Microscope Cryo-TEM	Krios G3i Cryo-TEM	Glacios Cryo-TEM
Source	X-FEG (high-brightness field emission gun)	
Accelerating voltage	300 kV	200 kV
Cryo-autoloader	Automated and contamination-free loading of cassettes (up to 12 Autogrids)	
Lenses	• Automatic condenser, objective, and SA apertures • Three-condenser-lens system for automated, continuous, and parallel sample illumination • Symmetric constant power C-TWIN objective lens with wide-gap pole piece (11 mm)	• Automatic condenser, objective, and SA apertures • Symmetric constant power objective lens (minimize image aberrations and lens hysteresis during mode switching) • Symmetric constant power C-TWIN objective lens with wide-gap pole piece (11 mm)
Stage	• Computerized 4-axis specimen stage with ±70-degree alpha tilt • Cryo-stage with single-axis holder for optimized stability and drift performance	• Computerized 4-axis specimen stage with ±70-degree alpha tilt • Cryo-stage with single-axis holder
Imaging	Rotation-free imaging with changing magnification	
Advanced performance monitoring	Self-assessment of optical microscope status, combined with automated alignments, ensuring that optimal experimental conditions are always available	
AFIS (aberration-free image shift)	Enhancing throughput with shorter relaxation times when moving coma-free between grid holes	
FFI (fringe-free imaging)	Enhanced throughput with multiple image acquisitions per grid hole	–
Software	Thermo Scientific: • EPU Software for single-particle analysis (SPA) screening and data acquisition • Tomography Software (cryo-ET)	Thermo Scientific: • EPU Software for single-particle analysis (SPA) screening and data acquisition • Tomography Software (cryo-ET) • EPU-D software
Detectors	• Falcon 4i Direct Electron Detector • Falcon 3 Direct Electron Detector • Thermo Scientific Ceta 16M • CMOS Camera	• Falcon 4 Direct Electron Detector • Thermo Scientific Ceta-D™Camera
Energy filter	Selectris Energy Filter	–
Other options	Thermo Scientific Phase Plate Solution	–

preserve macromolecules in a high vacuum of a transmission cryo-electron microscope, the sample needs to be vitrified, or in other words, freezing must happen fast enough to avoid crystalline ice formation. This is accomplished by rapidly plunging the grid with the applied sample solution into liquid ethane at a temperature below −135°C using semi-automated plungers. The optimal grid has particles trapped in a thin layer of amorphous ice, evenly dispersed and covering the full range of orientation distribution. Importantly, most often the quality of the sample undergoing vitrification is what determines whether high-resolution cryo-EM imaging and 3D reconstruction can be performed.

Once a sample has been vitrified, it is first examined using a diagnostic cryo-EM Glacios microscope (Table I) prior to any high-resolution data collection. At this stage, the specimen undergoes an initial evaluation in which several parameters are inspected, including ice thickness and homogeneity across the grid, overall ice quality, as well as protein integrity, concentration, stability, and spatial distribution — particularly with respect to potential aggregation or complex dissociation. The information obtained during this preliminary assessment is critical for adjusting grid preparation procedures so that the resulting grids meet the quality standards required for advanced data acquisition. If the sample demonstrates promising characteristics during this evaluation, additional images can be recorded to enable preliminary 2D and 3D processing (Fig. 2), resulting in an initial low- to intermediate-resolution map that can already allow for the identification of overall macromolecule architecture and domain organization. Once samples have been successfully screened and optimized, they may be transferred to the Krios G3i cryo-EM for data acquisition at the highest attainable resolution (Table I).

2.2. Data processing with SOLARIS cryo-EM

Single-particle analysis (SPA) datasets collected at the SOLARIS Cryo-EM Facility enable structural determination approaching near-atomic level details, typically reaching resolutions of $\approx$ 2 Å. Progressive improvements in 3D electron density maps obtained through successive rounds of data collection can be directly incorporated into downstream model-building programs, facilitating more accurate and detailed structural interpretation. A key aspect of cryo-EM image processing and generating the mentioned 3D density maps is that all images and reconstructions are transformed into Fourier space. In this reciprocal space, structural information is represented in terms of spatial frequencies, which facilitates efficient filtering, alignment, and three-dimensional reconstruction. Importantly, resolution estimation and validation are also performed in Fourier space. The final resolution of the cryo-EM map, defined as the global resolution of the reconstruction, is typically determined using the gold-standard Fourier shell correlation (GSFSC). In this method, the dataset is partitioned into two statistically independent subsets, each of which is processed separately to produce two independent, so-called half-maps. The level of agreement between these reconstructions is evaluated by calculating the Fourier shell correlation (FSC) as a function of spatial frequency. This yields a GSFSC curve, which serves as a reliable and cross-validated measure of resolution while reducing the likelihood of overfitting [9]. According to established cryo-EM standards, the final resolution is defined at the spatial frequency at which the GSFSC curve meets the 0.143 criterion [10].

The operating voltages of each microscope are explicitly listed in Table I. For each instrument, the acceleration voltage is fixed during standard operation. Experimental conditions are accordingly optimized to ensure high throughput and the highest attainable resolution for biological samples across a large user base.

The cryo-EM facility at the SOLARIS Centre is primarily dedicated to the structural characterization of biological samples and is specifically optimized for high-resolution single-particle analysis workflows. However, in response to specific user needs, the facility also provides access to complementary methodologies, including cryo-electron tomography (cryo-ET) and microcrystal electron diffraction (MicroED). These techniques extend the scope of structural investigations to different levels of structural organization.

Both microscopes, i.e., Krios G3i and Glacios, are equipped with highly stable automated goniometers with a single tilt axis, allowing for tilt angles up to $\pm 70°$. This angular range is essential for both tomographic data acquisition and three-dimensional electron diffraction (3DED) experiments. For 3DED, continuous-rotation data collection is supported, while dose-symmetric tilt schemes and multishot acquisition strategies are available for cryo-ET.

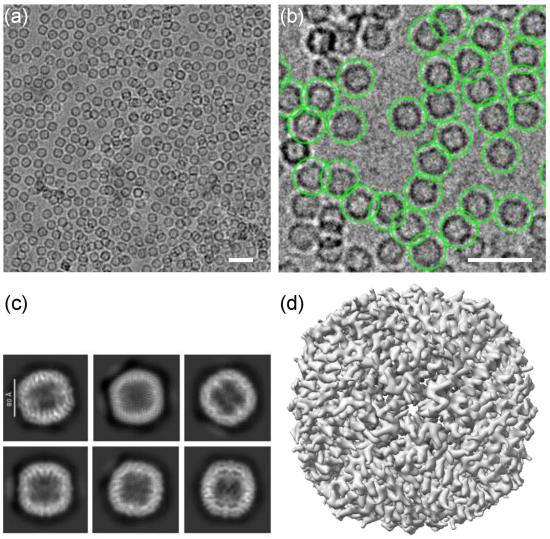

Fig. 2. Essential steps in cryo-EM SPA reconstruction: (a) averaged movie, (b) magnified view of particles chosen for extraction, (c) reference free 2D classes, (d) 3D macromolecule potential map; scale bar 20 nm.

3. Protein cages

3.1. Size and architecture

Protein cages, both naturally occurring and artificially designed, represent a diverse class of supramolecular assemblies with remarkable structural and functional properties. These cage-like structures are typically formed through the self-assembly of multiple protein subunits, resulting in a hollow interior that can encapsulate a variety of cargoes. Naturally occurring protein cages, such as viral capsids and ferritin, exhibit a wide range of sizes and architectures, reflecting their diverse roles in viral replication and iron storage. In recent years, there has been growing interest in the design and engineering of artificial protein cages for applications including drug delivery, vaccine development, and nanomaterial organization. The size and architecture of artificial protein cages can be precisely controlled through careful design of the protein subunits and their interactions. For example, TRAP-cages, constructed from ring-shaped protein subunits, can be engineered to form cages of different sizes and shapes by varying the number of subunits and their spatial arrangement [11–13]. Similarly, MS2 bacteriophage virus-like particles (VLPs) can be modified by inserting peptides into the capsid protein, resulting in the assembly of particles with larger sizes than the native form [14, 15].

3.2. Resolution and structural insights

The resolution of structural data is paramount to understanding the intricate details of biological assemblies, and advancements in cryo-EM have dramatically improved the achievable resolution in recent years. High-resolution structures, typically defined as those with a resolution of 4 Å or better, provide detailed information about the atomic arrangement of molecules, the nature of intermolecular interactions, and the conformational changes that occur during biological processes. In the context of protein cages, high-resolution structures can reveal the precise arrangement of protein subunits, the location and orientation of cargo molecules, and the structural features that govern cage assembly and disassembly. Sub-5 Å resolution structures of artificial protein cages with embedded gold nanoparticles have enabled detailed analysis of cage architecture and nanoparticle encapsulation. Furthermore, cryo-EM can be used to visualize assembly intermediates and defects, providing valuable insights into the mechanisms of cage formation. Beyond static structures, cryo-EM can also be used to study dynamic conformational changes in biological assemblies.

3.3. Mechanisms of cage assembly and disassembly

The mechanisms that govern the assembly and disassembly of protein cages are critical determinants of their function, particularly in applications such as drug delivery and cargo encapsulation. Many protein cages are designed to be stimuli-responsive, meaning that their assembly or disassembly can be triggered by external causes such as changes in pH, temperature, or the presence of specific molecules. Metal coordination is a versatile strategy for controlling the assembly and disassembly of protein cages. Programmable disassembly strategies can also be used to control the release of encapsulated cargoes. The precise mechanism of cargo encapsulation also plays a critical role in determining the efficiency and specificity of cargo delivery.

3.4. Applications of protein cages

The unique structural and functional properties of protein cages make them attractive candidates for a wide range of applications in biotechnology, medicine, and materials science. Their ability to encapsulate and protect cargo molecules, their tunable size and architecture, and their stimuli-responsive behavior make them particularly well-suited for drug delivery, vaccine development [14, 15], and nanomaterial organization [16].

4. RNA

4.1. Size and complexity of RNA molecules

Ribonucleic acid (RNA) is a versatile biological macromolecule that participates in various cellular processes, such as gene expression control or protein synthesis. RNA exhibits remarkable diversity in size and structure. This diversity arises from the unique chemical properties of RNA, its ability to form complex secondary and tertiary structures, and its capacity to hybridize with other nucleic acid molecules or interact with a wide range of proteins and other biomolecules. The size of RNA molecules varies widely, from 20 to 4000 nucleotides. Beyond their linear sequence, RNA molecules can adopt complex three-dimensional structures through the formation of base pairs, stacking interactions, and other non-covalent interactions. Post-transcriptional modifications further enhance the complexity and functional diversity of RNA molecules.

4.2. High-resolution structures of RNA and RNA–protein complexes

Determining the three-dimensional structures of free RNA molecules and their complexes with proteins is essential for understanding biological processes. While X-ray crystallography and NMR spectroscopy have been valuable tools for years, cryo-EM has emerged as a powerful technique for visualizing previously difficult to study RNA-protein assemblies. Cryo-EM has several advantages, including its ability to study molecules in their native state and the possibility of studying large, flexible, and heterogeneous complexes. Cryo-EM has revealed the structures of transfer RNAs (tRNAs) with various modifications, providing insights into how these modifications affect tRNA structure and function, the structures of RNA in complexes with modifying enzymes [17], as well as the structures of viral RNA genomes [18, 19].

4.3. Molecular mechanisms of RNA modification and function

Chemical modifications are essential for maintaining the structure, function, and role of RNA molecules. They affect a wide range of cellular processes. For example, m6A (N6-methyladenosine) is a prevalent modification in messenger RNA (mRNA) molecules [20]. If present in an mRNA codon, it slows down the translation process. This effect is counteracted by transfer RNAs (tRNA), whose wobble uridine is modified by Elongator, a large multi-subunit enzyme [21–23]. For this counteraction, tRNA thiolation, where the Uba4–Urm1

complex plays a role [24], is also needed. PUS3 is yet another modifying enzyme, a pseudouridine synthase that catalyzes the formation of pseudouridine at specific sites in tRNA molecules, mostly responsible for structure stabilisation [20, 21].

5. Enzyme complexes

5.1. Size and architecture of enzyme complexes

Some enzymes are multi-subunit assemblies that play essential roles in catalysing biochemical reactions within cells. They often consist of multiple protein subunits and require cofactors and regulatory proteins for their function. The size and architecture of enzyme complexes are critical determinants of their activity and regulation, influencing substrate binding and catalytic efficiency. The cytochrome b6f complex is a multi-subunit complex that participates in electron transfer between Photosystem II and Photosystem I [25, 26]. The eIF5A-DHS cryo-EM structure shows how eukaryotic translation initiation factor 5A (eIF5A) Lys50 undergoes the process of hypusination catalyzed by deoxyhypusine synthase (DHS) [27, 28].

5.2. Resolution and active site details

High-resolution structures provide invaluable insight into the active site architecture and catalytic mechanism of enzyme complexes. Cryo-EM has proven to be particularly useful in resolving the structural details of complex enzymes, enabling researchers to visualize substrate binding and transition states at the nearly-atomic level. High-resolution structures of cytochrome b6f showcase quinone binding sites [25, 26]. Human ELP123 structures, Elongator larger subcomplex, shed light on tRNA binding and anticodon unwinding to prepare wobble uridine for carboxymethylation at the 5th carbon position [16–18]. An eIF5A-DHS structure at 2.8 Å resolution explains the hypusination mechanism [27, 28].

5.3. Mechanisms of enzyme regulation

Enzyme activity is tightly regulated in response to cellular signals, ensuring that biochemical reactions are coordinated and appropriately modulated to meet the needs of the cell. The cytochrome b6f complex is regulated by a combination of substrate availability, inhibitor binding, and conformational changes [26]. The eIF5A-DHS complex, involved in hypusination of the eukaryotic translation initiation factor 5A (eIF5A), is regulated by the extracellular signal-regulated kinase 1/2 (ERK1/2) signaling pathway [28]. Allosteric regulation is a common mechanism for controlling enzyme activity. The SARS-CoV-2 methylation complex is subject to allosteric regulation [19].

5.4. Antibiotic resistance mechanism

Fighting antibiotic resistance is a burning issue in the scientific world. It drives research into novel strategies, for example, inhibiting essential cellular processes in bacteria. Albicidin, a peptide antibiotic, exhibits potent bactericidal activity by targeting deoxyribonucleic acid (DNA) gyrase through a dual-binding mechanism — one terminus disrupts the gyrase dimer interface, while the other intercalates into cleaved DNA, effectively locking the enzyme in a trapped state and preventing DNA religation. Cryo-EM structures of albicidin and its analogues reveal enhanced solubility and broadened activity against gyrase variants and topoisomerase IV, underscoring promise for last-resort therapeutic use [29]. In parallel, understanding bacterial uptake systems offers opportunities for precision delivery of antimicrobial peptides. Structural characterization of the SbmA and BacA transporters has uncovered a novel fold defining a family of SbmA-like peptide transporters. These secondary transporters utilize conserved glutamate residues for proton-driven translocation and feature an outward-open conformation with a large substrate-binding cavity, enabling promiscuous peptide uptake. Elucidation of this mechanism provides a foundation for designing narrow-spectrum antibiotics that exploit endogenous transport pathways [30].

6. Conclusions

Cryo-electron microscopy has revolutionized structural biology, enabling the determination of high-resolution structures of complex biological assemblies that were previously inaccessible. This review has highlighted the structural and functional diversity of complex biological assemblies revealed in collaboration with the NSRC SOLARIS Cryo-EM Facility. Presented cryo-EM studies of protein cages, RNA molecules, and enzyme complexes showcase the transformative impact of this technology and its benefit to the field of structural biology. In the realm of protein cages, cryo-EM has provided detailed insights into assembly, cargo encapsulation, and responses to external stimuli. In RNA biology, cryo-EM has enabled visualization of RNA molecules in their native state, revealing their complex structures and interactions with proteins. Cryo-EM has also provided invaluable insights into the structure and function of enzyme complexes, leading to a deeper understanding of essential cellular processes. While cryo-EM has proven to be a

powerful tool, its limitations must be acknowledged. One limitation is the relatively low throughput. Another is the difficulty of studying highly dynamic molecules. Despite these limitations, the future of cryo-EM is bright. Continued advancements are expected to further improve resolution and throughput. New methods for sample preparation are also expanding the range of samples that can be studied. As cryo-EM continues to evolve, it will undoubtedly play an increasingly important role in advancing our knowledge of complex biological systems and in developing new strategies for treating human diseases.

Acknowledgments

The cryo-EM facility at the National Synchrotron Radiation Centre is operational thanks to funding from the Ministry of Science and Higher Education under contract no. 1/SOL/2021/2.

References

[1] D. Cressey, E. Callaway, *Nature* **550**, 167 (2017).

[2] T.M. de Oliveira, L. van Beek, F. Shilliday, J.É. Debreczeni, C. Phillips, *SLAS Discov.* **26**, 17 (2021).

[3] A. Ignatiou, K. Macé, A. Redzej, T.R.D. Costa, G. Waksman, E.V. Orlova, in: *Bacterial Secretion Systems: Methods and Protocols*, *Methods in Molecular Biology*, Vol. 2715, Eds. L. Journet, E. Cascales, Springer, New York (NY) 2024, p. 431.

[4] A. Brown, S. Shao, *Curr. Opin. Struct. Biol.* **52**, 1 (2018).

[5] D. Zhu, D. Cao, X. Zhang, *Structure* **31**, 1348 (2023).

[6] W. Wang, *Genomics Appl. Biol.* **15**, 27 (2024).

[7] R. Henderson, *Q. Rev. Biophys.* **28**, 171 (1995).

[8] G. Ważny, M. Jaciuk, P. Indyka, S. Glatt, A. Biela, M. Rawski, *Ultramicroscopy* **283**, 114358 (2026).

[9] S.H.W Scheres, S. Chen, *Nat. Methods* **9**, 853 (2012).

[10] P.B. Rosenthal, R. Henderson, *J. Mol. Biol.* **333**, 721 (2003).

[11] I. Stupka, A.P. Biela, B. Piette, A. Kowalczyk, K. Majsterkiewicz, K. Borzęcka-Solarz, A. Naskalska, J.G. Heddle, *J. Mater. Chem. B* **12**, 436 (2023).

[12] I. Stupka, Y. Azuma, A.P. Biela, M. Imamura, S. Scheuring, E. Pyza, O. Woźnicka, D.P. Maskell, J.G. Heddle, *Sci. Adv.* **8**, eabj9424 (2022).

[13] N. Osiński, K. Majsterkiewicz, Z. Pakosz-Stępień, Y. Azuma, A.P. Biela, S. Gaweł, J.G. Heddle, *Macromol. Rapid. Commun.* **46**, 2400712 (2025).

[14] A.P. Biela, A. Naskalska, F. Fatehi, R. Twarock, J.G. Heddle, *Commun. Mater.* **3**, 7 (2022).

[15] A. Naskalska, M. Walczak, A. Dąbrowska, M. Bochenek, A. Biela, J. Heddle, *Int. J. Pharm.* **682**, 125865 (2025).

[16] K. Majsterkiewicz, A.P. Biela, S. Maity et al., *Nano Lett.* **22**, 3187 (2022).

[17] A.D. Biela, J.S. Nowak, A.P. Biela et al., *EMBO J.* **44**, 3553 (2025).

[18] T.R. de Moura, E. Purta, A. Bernat et al., *Nucl. Acids Res.* **52**, 3419 (2024).

[19] A. Matsuda, J. Plewka, M. Rawski et al., *Nucl. Acids Res.* **52**, 6441 (2024).

[20] S. Jain, L. Koziej, P. Poulis, I. Kaczmarczyk, M. Gaik, M. Rawski, N. Ranjan, S. Glatt, M.V. Rodnina, *Nat. Commun.* **14**, 4784 (2023).

[21] M.I. Dauden, M. Jaciuk, F. Weis et al., *Sci. Adv.* **5**, eaaw2326 (2019).

[22] N.-E.-H. Abbassi, M. Jaciuk, D. Scherf et al., *Nat. Commun.* **15**, 4094 (2024).

[23] M. Jaciuk, D. Scherf, K. Kaszuba et al., *Nucl. Acids Res.* **51**, 2011 (2023).

[24] M. Sokołowski, D. Kwasna, K.E. Ravichandran et al., *Nucl. Acids Res.* **52**, 13980 (2024).

[25] M. Sarewicz, M. Szwalec, S. Pintscher et al., *Sci. Adv.* **9**, eadd9688 (2023).

[26] S. Pintscher, R. Pietras, B. Mielecki et al., *Nat. Plants* **10**, 1814 (2024).

[27] E. Wątor, P. Wilk, A. Biela, M. Rawski, K.M. Zak, W. Steinchen, G. Bange, S. Glatt, P. Grudnik, *Nat. Commun.* **14**, 1689 (2023).

[28] A.E. Becker, P. Kochanowski, P.-K. Wu, E. Wątor, W. Chen, K. Guchhait, A.P. Biela, P. Grudnik, J.-I. Park, *Cell Rep.* **43**, 114831 (2024).

[29] E. Michalczyk, K. Hommernick, I. Behroz et al., *Nat. Catal.* **6**, 52 (2023).

[30] D. Ghilarov, S. Inaba-Inoue, P. Stepien et al., *Sci. Adv.* **7**, eabj5363 (2021).